Title
Multiparametric MR-PET measurements in hypermetabolic regions reflect differences in molecular status and tumor grade in treatment-naïve diffuse gliomas

Journal
Journal of Neuro-Oncology, 149(2)

ISSN
0167-594X

Authors
Tatekawa, Hiroyuki
Hagiwara, Akifumi
Uetani, Hiroyuki
et al.

Publication Date
2020-09-01

DOI
10.1007/s11060-020-03613-6

Peer reviewed

HHS Public Access

Author manuscript

J Neurooncol. Author manuscript; available in PMC 2021 September 14.

Published in final edited form as:

J Neurooncol. 2020 September ; 149(2): 337–346. doi:10.1007/s11060-020-03613-6.

Multiparametric MR-PET measurements in hypermetabolic regions reflect differences in molecular status and tumor grade in treatment-naïve diffuse gliomas

Hiroyuki Tatekawa[1,2], **Akifumi Hagiwara**[1,2], **Hiroyuki Uetani**[2], **Jingwen Yao**[1,2,3], **Talia C. Oughourlian**[1,2,4], **Shadfar Bahri**[5], **Chencai Wang**[1,2], **Catalina Raymond**[1,2], **Albert Lai**[6,7], **Timothy F. Cloughesy**[6,7], **Phioanh L. Nghiemphu**[6,7], **Linda M. Liau**[6,8], **Whitney B. Pope**[2], **Noriko Salamon**[2], **Benjamin M. Ellingson**[1,2,3,4,6]

[1.]UCLA Brain Tumor Imaging Laboratory (BTIL), Center for Computer Vision and Imaging Biomarkers, David Geffen School of Medicine, University of California Los Angeles, Los Angeles, USA

[2.]Department of Radiological Science, David Geffen School of Medicine, University of California Los Angeles, Los Angeles, USA

[3.]Department of Bioengineering, Henry Samueli School of Engineering, University of California Los Angeles, Los Angeles, USA

[4.]Neuroscience Interdepartmental Program, David Geffen School of Medicine, University of California Los Angeles, Los Angeles, USA

[5.]Department of Molecular and Medical Pharmacology, David Geffen School of Medicine, University of California Los Angeles, USA

Corresponding Author: Benjamin M. Ellingson, UCLA Brain Tumor Imaging Laboratory (BTIL), Center for Computer Vision and Imaging Biomarkers, David Geffen School of Medicine, University of California Los Angeles, Los Angeles, USA, Department of Radiological Science, David Geffen School of Medicine, University of California Los Angeles, Los Angeles, USA, 924 Westwood Blvd., Suite 615, Los Angeles, CA 90024 (bellingson@mednet.ucla.edu), Phone:(310)481-7572, Fax:(310)794-2796.

Authorship statement/contribution

Study design: Hiroyuki Tatekawa, Akifumi Hagiwara, Jingwen Yao, Noriko Salamon, Benjamin M. Ellingson. Acquisition: Albert Lai, Timothy F. Cloughesy, Phioanh L. Nghiemphu, Linda M. Liau. Image and data analysis: Hiroyuki Tatekawa, Akifumi Hagiwara, Hiroyuki Uetani, Jingwen Yao, Shadfar Bahri, Chencai Wang, Talia C. Oughourlian, Akifumi Hagiwara, Catalina Raymond, Noriko Salamon, Benjamin M. Ellingson. The first draft of the manuscript was written by Hiroyuki Tatekawa and all authors commented on previous versions of the manuscript. All authors read and approved the final manuscript and publication.

Conflicts of interest

Ellingson—Advisory Board— Hoffman La-Roche; Siemens; Nativis; Medicenna; MedQIA; Bristol-Myers Squibb; Imaging Endpoints; Agios. Paid Consultant—Nativis; MedQIA; Siemens; Hoffman La-Roche; Imaging Endpoints; Medicenna; Agios. Grant Funding—Hoffman La-Roche; Siemens; Agios; Janssen. Ellingson also holds a patent on this technology (US Patent #15/577,664; International PCT/US2016/034886). Cloughesy—Advisory Board—Roche/ Genentech, Amgen, Tocagen, NewGen, LPath, Proximagen, Celgene, Vascular Biogenics Ltd, Insys, Agios, Cortice Bioscience, Pfizer, Human Longevity, BMS, Merck, Notable Lab, MedQIA.

Ethics approval

All procedures performed in studies involving human participants were in accordance with the ethical standards of the institutional and/or national research committee and with the 1964 Helsinki declaration and its later amendments or comparable ethical standards. Written informed consent was obtained from all individual participants to have their imaging, clinical, and molecular data included in our research database (IRB IRB#10-000655).

[6]UCLA Neuro-Oncology Program, David Geffen School of Medicine, University of California Los Angeles, Los Angeles, USA

[7]Department of Neurology, David Geffen School of Medicine, University of California Los Angeles, Los Angeles, USA

[8]Department of Neurosurgery, David Geffen School of Medicine, University of California Los Angeles, Los Angeles, USA

Abstract

Purpose: To assess whether hypermetabolically-defined regions of interest (ROIs) on 3,4-dihydroxy-6-[18F]-fluoro-L-phenylalanine (FDOPA) positron emission tomography (PET) could be used to evaluate physiological features and whether there are measurable differences between molecular subtypes and tumor grades.

Methods: Sixty-eight treatment-naïve glioma patients who underwent FDOPA PET and magnetic resonance imaging (MRI) were retrospectively included. Fluid-attenuated inversion recovery hyperintense regions ($FLAIR_{ROI}$) were segmented. FDOPA hypermetabolic regions ($FDOPA_{ROI}$, tumor-to-striatum ratios > 1) within $FLAIR_{ROI}$ were extracted. Normalized maximum standardized uptake value ($nSUV_{max}$), volume of each ROI, and median relative cerebral blood volume (rCBV) and apparent diffusion coefficient (ADC) within $FLAIR_{ROI}$ or $FDOPA_{ROI}$ were calculated. Imaging metrics were compared using Students *t* or Mann-Whitney *U* tests. Area under the curve (AUC) of receiver-operating characteristic curves were used to determine whether imaging metrics within $FLAIR_{ROI}$ or $FDOPA_{ROI}$ can discriminate different molecular statuses or grades.

Results: Using either $FLAIR_{ROI}$ or $FDOPA_{ROI}$, the $nSUV_{max}$ and rCBV were significantly higher and the ADC was lower in isocitrate dehydrogenase [IDH] wild-type than mutant gliomas, and in higher-grade gliomas (HGGs) than lower-grade gliomas (LGGs). The $FDOPA_{ROI}$ volume was significantly higher in 1p19q codeleted than non-codeleted gliomas, and in HGGs than LGGs. Although not significant, imaging metrics extracted by $FDOPA_{ROI}$ discriminated molecular status and tumor grade more accurately than those extracted by $FLAIR_{ROI}$ (AUC of IDH status, 0.87 vs. 0.82; 1p19q status, 0.78 vs. 0.73; grade, 0.87 vs. 0.76).

Conclusion: FDOPA hypermetabolic ROI may extract useful imaging features of gliomas, which can illuminate biological differences between different molecular status or tumor grades.

Keywords

FDOPA PET; hypermetabolic ROI; glioma; MRI

Introduction

Recently, various advanced magnetic resonance imaging (MRI) sequences, including perfusion imaging, diffusion weighted imaging (DWI), spectroscopy, and functional MRI, can easily be acquired during a clinical examination to diagnose primary gliomas and evaluate their physiological features. Positron emission tomography (PET) using radiolabeled amino acids, including 3,4-dihydroxy-6-[18F]-fluoro-L-phenylalanine

(FDOPA), O-(2-[18F] fluoroethyl)-L-tyrosine (FET), and [11C] methyl-L-methionine, is often employed in neuro-oncological practice to identify metabolically active glioma tissue. FDOPA and FET PET have improved distribution and efficiency owing to the relatively long half-lives of fluorinated tracers (110 minutes) compared to carbon tracers (20 minutes). The use of FDOPA has grown rapidly especially in the United States, while that of FET has grown in Western Europe. Physiological MRI and amino acid PET can provide complementary metabolic information of gliomas [1].

For evaluation of MRI metrics, regions of interest (ROIs) of contrast-enhanced areas on T1-weighted images or hyperintense areas on T2-weighted/fluid-attenuated inversion recovery (FLAIR) images, referred to as anatomical ROIs, are most widely used for extracting representative features of physiological images. These anatomical delineation methods are also implemented in Response Assessment in Neuro-Oncology criteria for assessing tumor response to therapy [2, 3]. For evaluating amino acid PET metrics, the maximum standardized uptake value (SUV_{max}) is most commonly calculated using anatomical ROIs or visually placed spherical ROIs. Biological tumor volume (BTV), corresponding to hypermetabolic areas, and values of time-to-peak on dynamic PET studies are also extracted [4]. These multiparametric MRI and PET features were then compared between different tumor subtypes or World Health Organization (WHO) grades, integrated in regression analyses for differentiating groups or predicting prognoses [5, 6], and used as biomarkers for treatment responses [7].

Standard methods of creating ROIs have some limitations. Since not all gliomas, especially lower-grade gliomas (LGGs), show contrast enhancement, contrast-enhanced ROIs are generally applied to only images with higher-grade gliomas (HGGs), thus neglecting hypermetabolic areas of LGGs. Treatment-related changes, such as pseudoprogression and pseudoresponse, also affect the segmentation of contrast-enhanced ROIs. ROIs of FLAIR hyperintense regions can cover the whole tumors; however, these ROIs may include edema or hypoactive regions within gliomas, which may lead to misunderstanding of the biological activities of gliomas. Spherical ROIs can be manually overlaid on hypermetabolic areas on PET images; however, they potentially have a risk of selection bias, which may reduce reproducibility, and generally include a limited small area. Hence, there is a demand for developing a novel method to create unbiased but critical ROIs to extract specific imaging features of gliomas.

We hypothesized that extracting imaging metrics within FDOPA hypermetabolic ROIs may reflect unbiased physiological features within metabolically active gliomas. This method, to the best of our knowledge, has never been used for extracting MRI features. Although the molecular subtype and grade of gliomas were generally determined by resection or biopsy, clarifying imaging features of each subtype or grade of gliomas within metabolically active regions may help monitor therapeutic-related changes and predict prognosis later on. The objective of the current study was to assess whether hypermetabolically-defined ROIs on FDOPA PET could be used to evaluate tumor metabolism and whether there were measurable differences between molecular subtypes and tumor grades using this approach.

Materials and methods

Patient Selection

Overall, 68 patients with treatment-naïve and histologically confirmed gliomas who underwent FDOPA PET and MRI scans at our institution between 2007 and 2019 were retrospectively included. All patients were diagnosed with WHO grade II, III, or IV diffuse gliomas by surgical resection or biopsy according to the 2007 or 2016 WHO classification of the central nervous system tumors [8, 9]. The MRI scans were performed within 2 months of the corresponding PET scans. Patients were classified by isocitrate dehydrogenase (IDH) mutation status and 1p19q codeletion status, detected by conventional techniques [10]. When available, O6-methylguanine-DNA methyltransferase (MGMT) promoter methylation status and epidermal growth factor receptor (EGFR) amplification status were obtained. No patients underwent stereotactic biopsy prior to FDOPA PET or MRI. The study has been approved by the institutional review board, and all subjects signed an informed consent form. The same dataset was used in a previous study [11], which evaluated voxel-wise correlation between FDOPA and MRI.

FDOPA PET Image Acquisition

FDOPA PET images were acquired with a high-resolution full-ring PET/CT scanner (ECAT-HR; CTI/MIMVista; Siemens, Knoxville, TN, USA) after the subjects fasted for more than 4 hours. Using previously reported procedures, FDOPA was synthesized and injected intravenously [12, 13]. CT scans were performed prior to the PET scans for attenuation correction. Three-dimensional FDOPA emission data were acquired for a total of 30 minutes. The data were integrated between 10–30 minutes following the injection to obtain 20-minute static FDOPA images after reconstruction. FDOPA PET images were reconstructed using an ordered-subset expectation maximization iterative reconstruction algorithm, consisting of six iterations with eight subsets [14, 15]. Then a Gaussian filter with a full width at half maximum of 4 mm was applied, resulting in voxel sizes of 1.34 × 1.34 × 3 mm. SUV maps of FDOPA were calculated based on the radioactive activity divided by the decay-corrected injected dose per body mass [16]. The resulting SUV maps were normalized (nSUV) relative to the median value of the contralateral healthy striatum [10, 17].

Magnetic Resonance Image Acquisition

Anatomical MRI consisted at least of standard T1-weighted pre- and post-contrast images at 2D axial turbo spin echo with 3 mm slice thickness and no interslice gap or 3D inversion prepared gradient echo images with 1–1.5 mm isotropic voxel size. FLAIR images were acquired at 3 mm slice thickness with no interslice gap using a 1.5-T or 3-T clinical MRI scanner.

For dynamic susceptibility contrast (DSC) perfusion MRI, a total dose of 0.1 mmol/kg of Gd-DTPA or Gd-BTDO3A (Magnevist or Gadavist; Bayer Healthcare Pharmaceuticals, Wayne, NJ, USA) was administered with 0.025 mmol/kg for the preload dosage to mitigate T1-based leakage contamination. The remaining 0.075 mmol/kg was used for dynamic bolus administration as previously described [18]. A two-minute gap was placed between the

preload dose and the initiation of the baseline DSC-MRI. The DSC-MRI was acquired with slice thickness = 5 mm with no interslice gap, number of baseline acquisitions before contrast agent injection = 10–25, and number of timepoints =120. First, dynamic time-series images were motion-corrected using FSL software (*mcflirt*; FMRIB, Oxford, UK; http://www.fmrib.ox.ac.uk/fsl/). Second, relative cerebral blood volume (rCBV) maps were calculated using a bidirectional contrast agent leakage-correction algorithm to model contrast flux into and out of the vasculature [19]. Finally, a normalized rCBV map was computed by dividing the rCBV map by the median rCBV value of the contralateral normal-appearing white matter.

DWI was performed prior to injection of contrast agent using a single-shot echo-planar imaging sequence in the axial plane for nine patients, and was acquired with slice thickness of 3 mm with no interslice gap. ADC maps were calculated from the acquired DWI with b = 1000 s/mm^2 and b = 0 s/mm^2 images, and expressed in units of 10^{-6} mm^2/sec. Diffusion tensor imaging (DTI) data was collected for 54 patients for whom conventional DWI was not obtained, and mean diffusivity maps were used as estimates of ADC values after motion-correction using FSL software (*eddy* and *dtifit*). The parameter of the DTI consisted of 12–64 equidistant diffusion-sensitizing directions with b = 1000 s/mm^2, along with a single b = 0 s/mm^2 image with slice thickness of 2–3 mm with no interslice gap.

Postprocessing and ROI Analysis

All MRI and PET images were registered to the post-contrast T1-weighted images for each patient using a six-degree of freedom rigid transformation and a mutual information cost function using FSL software (*flirt*) or Freesurfer software (*tkregister2*; Massachusetts General Hospital, Harvard Medical School, MA, USA; https://surfer.nmr.mgh.harvard.edu). To register the ADC maps, we rigidly aligned b = 0 s/mm^2 images acquired during the DWI or DTI sequence to the post-contrast T1-weighted images and applied the transform matrix to the ADC maps. A single ROI was segmented based on the region of hyperintensity on T2-weighted FLAIR as $FLAIR_{ROI}$ by a board-certificated neuroradiologist (H.T. with 13 years of clinical experience) with Analysis of Functional Neuroimages software (AFNI; NIMH Scientific and Statistical Computing Core; Bethesda, MD, USA; https://afni.nimh.nih.gov) using a semi-automatic procedure as previously described [20, 21]. Maximum nSUV ($nSUV_{max}$) was quantified within $FLAIR_{ROI}$. Also, a FDOPA hypermetabolic area (voxels with tumor-to-striatum ratios > 1) within $FLAIR_{ROI}$ was extracted as $FDOPA_{ROI}$, which is equivalent to BTV. This cut-off of one was determined according to the previous suggestion [17, 22]. The volumes of $FLAIR_{ROI}$ and $FDOPA_{ROI}$ were measured in milliliters. Median rCBV and median ADC within $FLAIR_{ROI}$ or $FDOPA_{ROI}$ were also calculated separately. Figure 1 illustrates an example of segmentations of $FLAIR_{ROI}$ and $FDOPA_{ROI}$ in a 74-year-old male glioblastoma patient.

Statistical Analyses

The Shapiro-Wilk test was used to test for normality. Student's *t*-tests and Mann-Whitney *U* tests were performed for normally and non-normally distributed data, respectively.

The following comparisons were performed between different IDH status (IDH wild-type [IDH_{wt}] vs. IDH mutant [IDH_m]), 1p19q codeletion status (non-codeleted vs. codeleted for IDH_m gliomas), MGMT methylation status (unmethylated vs. methylated), EGFR amplification status (negative vs. positive), and tumor grade (LGGs [grade II] vs. HGGs [grade III and IV]). For evaluating MRI and PET metrics, a total of seven imaging metrics including $nSUV_{max}$, $FLAIR_{ROI}$ volume, $FDOPA_{ROI}$ volume, median rCBV within $FLAIR_{ROI}$ and $FDOPA_{ROI}$, and median ADC within $FLAIR_{ROI}$ and $FDOPA_{ROI}$ were compared between different glioma groups.

For evaluating the discriminatory potential, a multiple logistic regression model was used to differentiate molecular statuses and tumor grades. The variables extracted by $FLAIR_{ROI}$ or $FDOPA_{ROI}$ were separately integrated into the regression models. Imaging variables calculated by $FLAIR_{ROI}$ included $FLAIR_{ROI}$ volume, median rCBV within $FLAIR_{ROI}$, and median ADC within $FLAIR_{ROI}$. Imaging variable calculated by $FDOPA_{ROI}$ included $FDOPA_{ROI}$ volume, median rCBV within $FDOPA_{ROI}$, and median ADC within $FDOPA_{ROI}$. The $nSUV_{max}$ was additionally integrated as a single variable or to the imaging variables extracted by $FDOPA_{ROI}$. Receiver-operating characteristic (ROC) curves were used to determine whether each method could discriminate molecular statuses and tumor grades. The area under the curve (AUC) of ROC curve and the sensitivity and specificity of discrimination were evaluated as measures of model performance. Comparison between the ROC curves calculated by $FLAIR_{ROI}$ and those calculated by $FDOPA_{ROI}$ was also performed.

Statistical analyses were performed using R software (version 3.5.2; http://www.r-project.org/) and GraphPad Prism (Version 8.3; GraphPad Software, La Jolla, CA). Statistical significance was defined as $P < 0.05$.

Results

Overall, 68 treatment-naïve glioma patients (n = 26 female) with a mean age of 51.7 (standard deviation, 14.9) years at the time of PET examination were included (TABLE 1 and Supplemental TABLE 1). Perfusion imaging and DWI for 61 and 63 patients with clinically useful quality were obtained. All patients were evaluated using $FLAIR_{ROI}$, while 53 of the 68 included patients were evaluated using $FDOPA_{ROI}$, because the $nSUV_{max}$ of gliomas in 15 patients (IDH_{wt}: n = 2 grade II, n = 3 grade III, n = 1 grade IV; IDH_m non-codeleted: n = 4 grade II, n = 2 grade III; IDH_m codeleted: n = 3 grade II) were less than the threshold of one.

Figure 2 demonstrates the results comparing IDH_{wt} (n = 36) and IDH_m gliomas (n = 32). The $nSUV_{max}$ was significantly higher in IDH_{wt} than in IDH_m gliomas ($P = 0.034$). The rCBV within both $FLAIR_{ROI}$ and $FDOPA_{ROI}$ were significantly higher ($P = 0.007$ and < 0.001, respectively) and ADC within $FLAIR_{ROI}$ and $FDOPA_{ROI}$ were significantly lower (both $Ps < 0.001$) in IDH_{wt} than in IDH_m gliomas. The imaging metrics calculated by $FDOPA_{ROI}$ showed better discrimination ability of IDH status (AUC, 0.87; sensitivity, 100%; specificity, 65%) compared with those calculated by $FLAIR_{ROI}$ (AUC, 0.82;

sensitivity, 89%; specificity, 66%). When $nSUV_{max}$ was included, discrimination was further improved (AUC, 0.91; sensitivity, 90%; specificity, 87%).

Figure 3 summarizes the results comparing IDH_m 1p19q non-codeleted (n = 16) and IDH_m 1p19q codeleted gliomas (n = 16). The $FDOPA_{ROI}$ volume was significantly higher in codeleted than non-codeleted gliomas ($P = 0.022$). The rCBV within $FLAIR_{ROI}$ was significantly higher in codeleted than non-codeleted gliomas ($P = 0.044$). The imaging metrics calculated by $FDOPA_{ROI}$ (AUC, 0.78; sensitivity, 56%; specificity, 100%) showed better discrimination ability of 1p19q codeletion status compared with those calculated by $FLAIR_{ROI}$ (AUC, 0.73; sensitivity, 64%; specificity, 81%). When $nSUV_{max}$ was included, discrimination was further improved (AUC, 0.83; sensitivity, 67%; specificity, 100%).

The results of MGMT and EGFR status are described in Supplemental Figures 1 and 2.

Figure 4 summarizes comparisons between LGGs (n = 29 grade II) and HGGs (n = 39 grade III and IV). The $nSUV_{max}$ and $FDOPA_{ROI}$ volume were significantly higher in HGGs than LGGs ($P < 0.001$ and 0.003, respectively). The rCBV within both $FLAIR_{ROI}$ and $FDOPA_{ROI}$ were significantly higher ($P = 0.049$ and < 0.001, respectively) and ADC within $FLAIR_{ROI}$ and $FDOPA_{ROI}$ were significantly lower ($P = 0.001$ and < 0.001, respectively) in HGGs than LGGs. The imaging metrics calculated by $FDOPA_{ROI}$ (AUC, 0.87; sensitivity, 76%; specificity, 88%) exhibited a better ability to discriminate tumor grade compared with those calculated by $FLAIR_{ROI}$ (AUC, 0.76; sensitivity, 69%; specificity, 83%). When $nSUV_{max}$ was included, discrimination was further improved (AUC, 0.89; sensitivity, 76%; specificity, 94%).

No ROC curve pairs calculated by $FLAIR_{ROI}$ and $FDOPA_{ROI}$ showed significant differences in the differentiation of IDH status, 1p19q status, nor tumor grade. The prediction abilities of each group for independent imaging metrics are shown in Supplemental Figure 3. When comparing the ROC curves of independent imaging metrics, only rCBV within $FDOPA_{ROI}$ had a significantly better discrimination ability for tumor grade than rCBV within $FLAIR_{ROI}$ (AUC: 0.85 vs. 0.65; $P = 0.030$).

Discussion

In this study we found that imaging metrics calculated by $FDOPA_{ROI}$ exhibited improved discrimination between different molecular statuses and tumor grades than those calculated by $FLAIR_{ROI}$. These findings suggested that imaging metrics within metabolically active regions may capture more useful features of gliomas than those within anatomical ROIs.

FDOPA hypermetabolic areas referred to as BTV were used as ROIs for calculating physiological MRI metrics in this study. The threshold of FDOPA hypermetabolism was defined as the median value of the basal ganglia, which has been empirically used for FDOPA examinations [17, 22]. PET-derived delineation of a tumor is useful for evaluating responses to molecular targeted therapy and chemotherapy [7, 23, 24], and for predicting prognosis after chemoradiotherapy [25], regardless of contrast enhancement. Prior to this study, BTV had never been used as a ROI for calculating other imaging metrics, such as those from physiologic MRI. We hypothesized that our method using hypermetabolic ROIs

could focus on hypermetabolic areas with high reproducibility, and mitigate confounding factors such as necrosis, bleeding, and edema within tumors, resulting in more accurate characterization of biologically active areas of gliomas [26]. However, the limitation of hypermetabolic ROIs is that the $nSUV_{max}$ must be higher than the threshold. In line with a previous study reporting that about 30% of newly diagnosed gliomas were PET-negative against the background of amino acid PET [27], we chose to exclude 15 of the 68 (22%) gliomas for the evaluations using $FDOPA_{ROI}$ due to their hypometabolism. Meanwhile, hypermetabolic ROIs may be useful when gliomas are suspected following standard MRI, and thereafter revealed to be amino acid PET-positive. In such cases, our new technique may extract more useful features of gliomas than the widely used standard technique using $FLAIR_{ROI}$. The hypermetabolic ROI used in this study may also be applicable to other PET tracers; hence, validation in other tracers is desired.

Diffuse gliomas were previously classified into astrocytomas, oligodendrogliomas, and oligoastrocytomas, ranging from WHO grade II to grade IV according to their histologic features. In 2016, the WHO classification of Tumors of the Central Nervous System reclassified gliomas by integrating molecular status, such as IDH gene mutation and chromosomal 1p19q co-deletion, as well as histologic characteristics [9]. Thereafter, for the treatment of gliomas, main interests related to the management and prognostication reside in IDH mutation status. Patients with IDH_m gliomas often exhibit relatively favorable outcomes, while IDH_{wt} gliomas often lead to poor prognosis [28]. In this study, IDH_{wt} gliomas showed higher $nSUV_{max}$, hypermetabolic volume, and rCBV and lower ADC than IDH_m gliomas for both $FLAIR_{ROI}$ and $FDOPA_{ROI}$. Although a previous study comparing LGGs with IDH_{wt} and IDH_m showed higher $nSUV_{max}$ in IDH_m gliomas [29], this study showed higher $nSUV_{max}$ in IDH_{wt} gliomas, which may be partly due to that all grade IV gliomas in this study were IDH_{wt}. Glioma grading is important in prognostication and in making treatment decisions. Increased FDOPA uptake predicted not only higher tumor grade, but worse outcomes [5]. This study revealed higher $nSUV_{max}$, hypermetabolic volumes, and rCBV, and lower ADC in HGGs than LGGs for both $FLAIR_{ROI}$ and $FDOPA_{ROI}$. These results between different tumor grades are consistent with those from the previous study [4]. When evaluating the diagnostic performance, imaging metrics extracted by $FDOPA_{ROI}$ improved discrimination compared with those extracted by $FLAIR_{ROI}$, suggesting that imaging metrics extracted by hypermetabolic ROIs may illuminate biological differences between different subtypes or tumor grades.

This study was subject to some limitations. First, although hypermetabolic ROI used in this study may be useful to extract imaging features within the hypermetabolic region with high reproducibility, amino acid PET uptake values within the ROIs must be higher than the thresholds. Second, although this study showed better AUC to differentiate IDH status, 1p19q status, and tumor grade by using $FDOPA_{ROI}$ rather than $FLAIR_{ROI}$, the comparison of ROC curves using different methods did not significantly differ. Further validation in a larger population is required. Third, the patient age and sex may affect the FDOPA uptake in the background of the brain structures [30]; however, this study did not adjust for these factors. Fourth, due to the retrospective nature, the acquisition parameters and scanners of MRI were not identical across patients, and perfusion imaging and DWI were not acquired for all patients. A prospective study is needed to fully elucidate the potential of our novel

technique in management of gliomas. Lastly, this study did not use contrast-enhanced regions as ROIs nor for volumetry because only one third of the gliomas in this study showed contrast enhancement (IDH_{wt}, 16/36; $IDH_{m\text{-}non\text{-}codel}$, 4/16; $IDH_{m\text{-}codel}$, 2/16; HGGs, 18/39; LGGs, 4/29). However, evaluation of the associations or differences between contrast-enhanced ROIs and FDOPA hypermetabolic ROIs may reveal new aspects of gliomas, especially for IDH_{wt} gliomas and HGGs.

Conclusion

FDOPA hypermetabolic ROI may extract useful, unbiased imaging features of gliomas, which can be used to illuminate biological differences between different molecular status and tumor grades, and lead to the discovery of novel imaging biomarkers.

Supplementary Material

Refer to Web version on PubMed Central for supplementary material.

Acknowledgments

Funding

Grant from the Society of Nuclear Medicine and Molecular Imaging (SNMMI) (Tatekawa); American Cancer Society (ACS) Research Scholar Grant (RSG-15-003-01-CCE) (Ellingson); American Brain Tumor Association (ABTA) Research Collaborators Grant (ARC1700002) (Ellingson); National Brain Tumor Society (NBTS) Research Grant (Ellingson, Cloughesy); NIH/NCI UCLA Brain Tumor SPORE (1P50CA211015-01A1) (Ellingson, Lai, Cloughesy, Nghiemphu); NIH/NCI 1R21CA223757-01 (Ellingson)

References

1. Galldiks N, Lohmann P, Cicone F, Langen KJ (2019) FET and FDOPA PET Imaging in Glioma In: Pope W (ed) Glioma Imaging. 1st edn. Springer, Switzerland, pp 211–222
2. Ellingson BM, Wen PY, Cloughesy TF (2017) Modified Criteria for Radiographic Response Assessment in Glioblastoma Clinical Trials. Neurotherapeutics 14: 307–320 doi:10.1007/s13311-016-0507-6 [PubMed: 28108885]
3. Wen PY, Macdonald DR, Reardon DA, Cloughesy TF, Sorensen AG, Galanis E, Degroot J, Wick W, Gilbert MR, Lassman AB, Tsien C, Mikkelsen T, Wong ET, Chamberlain MC, Stupp R, Lamborn KR, Vogelbaum MA, van den Bent MJ, Chang SM (2010) Updated response assessment criteria for high-grade gliomas: response assessment in neuro-oncology working group. J Clin Oncol 28: 1963–1972 doi:10.1200/JCO.2009.26.3541 [PubMed: 20231676]
4. Vettermann F, Suchorska B, Unterrainer M, Nelwan D, Forbrig R, Ruf V, Wenter V, Kreth FW, Herms J, Bartenstein P, Tonn JC, Albert NL (2019) Non-invasive prediction of IDH-wildtype genotype in gliomas using dynamic (18)F-FET PET. Eur J Nucl Med Mol Imaging 46: 2581–2589 doi:10.1007/s00259-019-04477-3 [PubMed: 31410540]
5. Patel CB, Fazzari E, Chakhoyan A, Yao J, Raymond C, Nguyen H, Manoukian J, Nguyen N, Pope W, Cloughesy TF, Nghiemphu PL, Czernin J, Lai A, Ellingson BM (2018) (18)F-FDOPA PET and MRI characteristics correlate with degree of malignancy and predict survival in treatment-naive gliomas: a cross-sectional study. J Neurooncol 139: 399–409 doi:10.1007/s11060-018-2877-6 [PubMed: 29679199]
6. Floeth FW, Pauleit D, Sabel M, Stoffels G, Reifenberger G, Riemenschneider MJ, Jansen P, Coenen HH, Steiger HJ, Langen KJ (2007) Prognostic value of O-(2-18F-fluoroethyl)-L-tyrosine PET and MRI in low-grade glioma. J Nucl Med 48: 519–527 doi:10.2967/jnumed.106.037895 [PubMed: 17401087]

7. Suchorska B, Unterrainer M, Biczok A, Sosnova M, Forbrig R, Bartenstein P, Tonn JC, Albert NL, Kreth FW (2018) (18)F-FET-PET as a biomarker for therapy response in non-contrast enhancing glioma following chemotherapy. J Neurooncol 139: 721–730 doi:10.1007/s11060-018-2919-0 [PubMed: 29948765]
8. Louis DN, Ohgaki H, Wiestler OD, Cavenee WK, Burger PC, Jouvet A, Scheithauer BW, Kleihues P (2007) The 2007 WHO classification of tumours of the central nervous system. Acta Neuropathol 114: 97–109 doi:10.1007/s00401-007-0243-4 [PubMed: 17618441]
9. Louis DN, Perry A, Reifenberger G, von Deimling A, Figarella-Branger D, Cavenee WK, Ohgaki H, Wiestler OD, Kleihues P, Ellison DW (2016) The 2016 World Health Organization Classification of Tumors of the Central Nervous System: a summary. Acta Neuropathol 131: 803–820 doi:10.1007/s00401-016-1545-1 [PubMed: 27157931]
10. Oughourlian TC, Yao J, Schlossman J, Raymond C, Ji M, Tatekawa H, Salamon N, Pope WB, Czernin J, Nghiemphu PL, Lai A, Cloughesy TF, Ellingson BM (2020) Rate of change in maximum (18)F-FDOPA PET uptake and non-enhancing tumor volume predict malignant transformation and overall survival in low-grade gliomas. J Neurooncol 147: 135–145 doi:10.1007/s11060-020-03407-w [PubMed: 31981013]
11. Tatekawa H, Hagiwara A, Yao J, Oughourlian TC, Ueda I, Uetani H, Raymond C, Lai A, Cloughesy TF, Nghiemphu PL, Liau LM, Pope WB, Salamon N, Ellingson BM (2020) Voxel-wise and patient-wise correlation of 18F-FDOPA PET, rCBV, and ADC in treatment-naïve diffuse gliomas with different molecular subtypes. J Nucl Med
12. Bishop A, Satyamurthy N, Bida G, Hendry G, Phelps M, Barrio JR (1996) Proton irradiation of [18O]O2: production of [18F]F2 and [18F]F2 + [18F] OF2. Nucl Med Biol 23: 189–199 doi:10.1016/0969-8051(95)02037-3 [PubMed: 8782226]
13. Namavari M, Bishop A, Satyamurthy N, Bida G, Barrio JR (1992) Regioselective radiofluorodestannylation with [18F]F2 and [18F]CH3COOF: a high yield synthesis of 6-[18F]Fluoro-L-dopa. Int J Rad Appl Instrum A 43: 989–996 doi:10.1016/0883-2889(92)90217-3 [PubMed: 1330984]
14. Kinahan PE, Townsend DW, Beyer T, Sashin D (1998) Attenuation correction for a combined 3D PET/CT scanner. Med Phys 25: 2046–2053 doi:10.1118/1.598392 [PubMed: 9800714]
15. Nuyts J, Michel C, Dupont P (2001) Maximum-likelihood expectation-maximization reconstruction of sinograms with arbitrary noise distribution using NEC-transformations. IEEE Trans Med Imaging 20: 365–375 doi:10.1109/42.925290 [PubMed: 11403196]
16. Thie JA (2004) Understanding the standardized uptake value, its methods, and implications for usage. J Nucl Med 45: 1431–1434 [PubMed: 15347707]
17. Chen W, Silverman DH, Delaloye S, Czernin J, Kamdar N, Pope W, Satyamurthy N, Schiepers C, Cloughesy T (2006) 18F-FDOPA PET imaging of brain tumors: comparison study with 18F-FDG PET and evaluation of diagnostic accuracy. J Nucl Med 47: 904–911 [PubMed: 16741298]
18. Wang YL, Yao J, Chakhoyan A, Raymond C, Salamon N, Liau LM, Nghiemphu PL, Lai A, Pope WB, Nguyen N, Ji M, Cloughesy TF, Ellingson BM (2019) Association between Tumor Acidity and Hypervascularity in Human Gliomas Using pH-Weighted Amine Chemical Exchange Saturation Transfer Echo-Planar Imaging and Dynamic Susceptibility Contrast Perfusion MRI at 3T. AJNR Am J Neuroradiol 40: 979–986 doi:10.3174/ajnr.A6063 [PubMed: 31097430]
19. Leu K, Boxerman JL, Lai A, Nghiemphu PL, Pope WB, Cloughesy TF, Ellingson BM (2016) Bidirectional Contrast agent leakage correction of dynamic susceptibility contrast (DSC)-MRI improves cerebral blood volume estimation and survival prediction in recurrent glioblastoma treated with bevacizumab. J Magn Reson Imaging 44: 1229–1237 doi:10.1002/jmri.25227 [PubMed: 26971534]
20. Ellingson BM, Kim HJ, Woodworth DC, Pope WB, Cloughesy JN, Harris RJ, Lai A, Nghiemphu PL, Cloughesy TF (2014) Recurrent glioblastoma treated with bevacizumab: contrast-enhanced T1-weighted subtraction maps improve tumor delineation and aid prediction of survival in a multicenter clinical trial. Radiology 271: 200–210 doi:10.1148/radiol.13131305 [PubMed: 24475840]
21. Tran AN, Lai A, Li S, Pope WB, Teixeira S, Harris RJ, Woodworth DC, Nghiemphu PL, Cloughesy TF, Ellingson BM (2014) Increased sensitivity to radiochemotherapy in IDH1 mutant

glioblastoma as demonstrated by serial quantitative MR volumetry. Neuro Oncol 16: 414–420 doi:10.1093/neuonc/not198 [PubMed: 24305712]

22. Law I, Albert NL, Arbizu J, Boellaard R, Drzezga A, Galldiks N, la Fougere C, Langen KJ, Lopci E, Lowe V, McConathy J, Quick HH, Sattler B, Schuster DM, Tonn JC, Weller M (2019) Joint EANM/EANO/RANO practice guidelines/SNMMI procedure standards for imaging of gliomas using PET with radiolabelled amino acids and [(18)F]FDG: version 1.0. Eur J Nucl Med Mol Imaging 46: 540–557 doi:10.1007/s00259-018-4207-9 [PubMed: 30519867]
23. Harris RJ, Cloughesy TF, Pope WB, Nghiemphu PL, Lai A, Zaw T, Czernin J, Phelps ME, Chen W, Ellingson BM (2012) 18F-FDOPA and 18F-FLT positron emission tomography parametric response maps predict response in recurrent malignant gliomas treated with bevacizumab. Neuro Oncol 14: 1079–1089 doi:10.1093/neuonc/nos141 [PubMed: 22711609]
24. Roelcke U, Wyss MT, Nowosielski M, Ruda R, Roth P, Hofer S, Galldiks N, Crippa F, Weller M, Soffietti R (2016) Amino acid positron emission tomography to monitor chemotherapy response and predict seizure control and progression-free survival in WHO grade II gliomas. Neuro Oncol 18: 744–751 doi:10.1093/neuonc/nov282 [PubMed: 26578622]
25. Suchorska B, Jansen NL, Linn J, Kretzschmar H, Janssen H, Eigenbrod S, Simon M, Pöpperl G, Kreth FW, la Fougere C, Weller M, Tonn JC (2015) Biological tumor volume in 18FET-PET before radiochemotherapy correlates with survival in GBM. Neurology 84: 710–719 doi:10.1212/wnl.0000000000001262 [PubMed: 25609769]
26. Karavaeva E, Harris RJ, Leu K, Shabihkhani M, Yong WH, Pope WB, Lai A, Nghiemphu PL, Liau LM, Chen W, Czernin J, Cloughesy TF, Ellingson BM (2015) Relationship Between [18F]FDOPA PET Uptake, Apparent Diffusion Coefficient (ADC), and Proliferation Rate in Recurrent Malignant Gliomas. Mol Imaging Biol 17: 434–442 doi:10.1007/s11307-014-0807-3 [PubMed: 25465392]
27. Xiao J, Jin Y, Nie J, Chen F, Ma X (2019) Diagnostic and grading accuracy of (18)F-FDOPA PET and PET/CT in patients with gliomas: a systematic review and meta-analysis. BMC Cancer 19: 767 doi:10.1186/s12885-019-5938-0 [PubMed: 31382920]
28. Gittleman H, Sloan AE, Barnholtz-Sloan JS (2019) An independently validated survival nomogram for lower grade glioma. Neuro Oncol doi:10.1093/neuonc/noz191
29. Verger A, Metellus P, Sala Q, Colin C, Bialecki E, Taieb D, Chinot O, Figarella-Branger D, Guedj E (2017) IDH mutation is paradoxically associated with higher (18)F-FDOPA PET uptake in diffuse grade II and grade III gliomas. Eur J Nucl Med Mol Imaging 44: 1306–1311 doi:10.1007/s00259-017-3668-6 [PubMed: 28293705]
30. Cicone F, Carideo L, Minniti G, Scopinaro F (2019) The mean striatal (18)F-DOPA uptake is not a reliable cut-off threshold for biological tumour volume definition of glioma. Eur J Nucl Med Mol Imaging 46: 1051–1053 doi:10.1007/s00259-019-4276-4 [PubMed: 30685796]

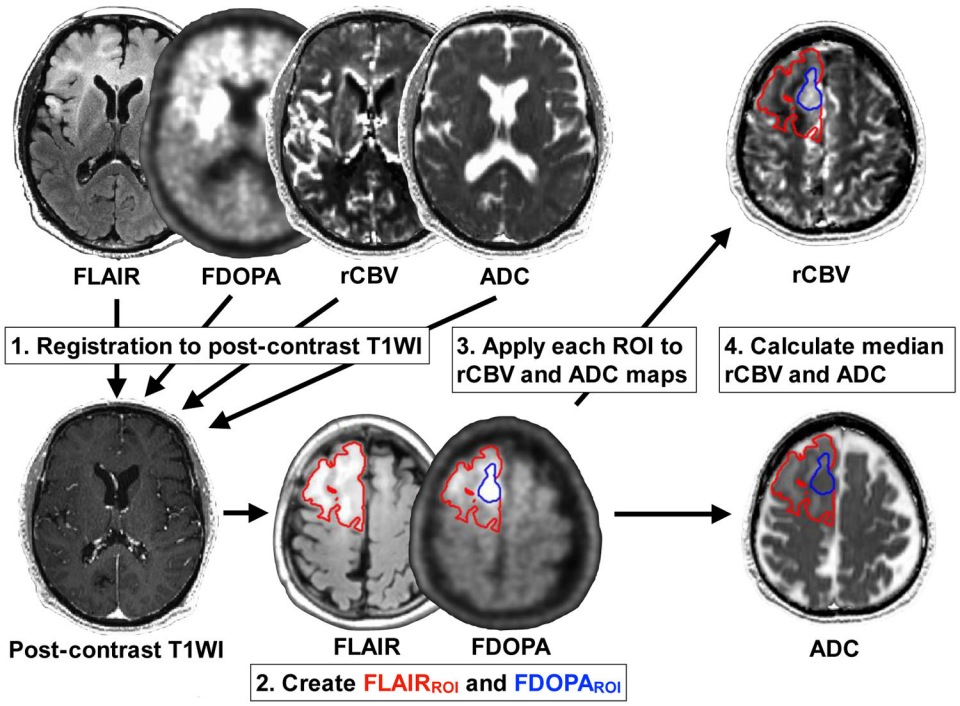

Fig. 1.

An example of post-processing on a 74-year-old male patient with a WHO grade IV, IDH wild-type, MGMT-unmethylated, and EGFR amplification-negative glioblastoma. After registration of all images to post-contrast T1-weighted images, an ROI of FLAIR hyperintensity is segmented ($FLAIR_{ROI}$: red area), and applied to FDOPA PET images. FDOPA hypermetabolic region ($FDOPA_{ROI}$: blue area) higher than the striatum within $FLAIR_{ROI}$ is extracted. The $nSUV_{max}$ within $FLAIR_{ROI}$ and volume of each ROI are calculated. $FLAIR_{ROI}$ and $FDOPA_{ROI}$ are applied to rCBV and ADC maps, and median rCBV and ADC within each ROI are calculated

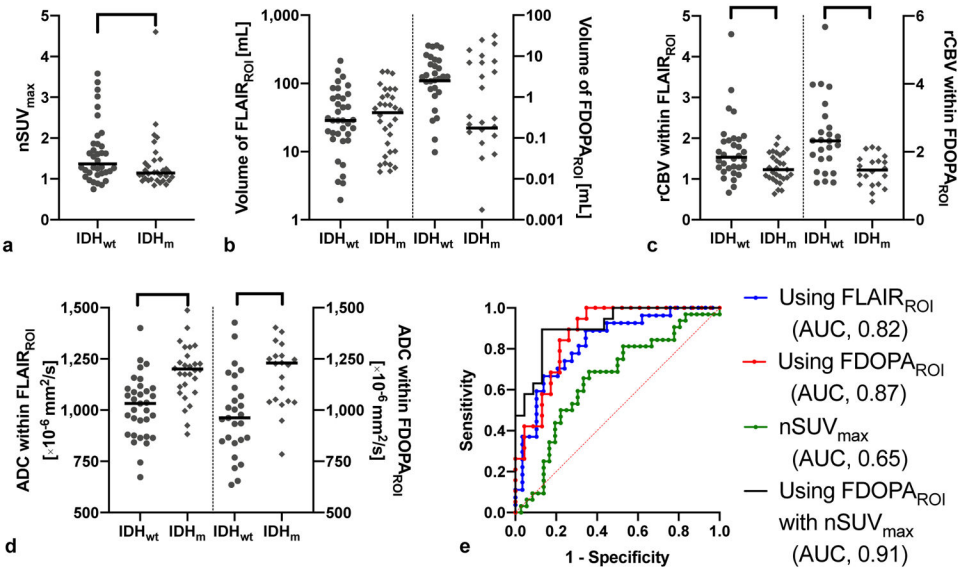

Fig. 2.

Imaging metrics of FDOPA PET and MRI, and the ROC curve in IDH_{wt} (n = 36) and IDH_m (n = 32). a) The $nSUV_{max}$ is significantly higher in IDH_{wt} than IDH_m gliomas. b) The volume of $FLAIR_{ROI}$ and $FDOPA_{ROI}$ do not significantly differ. c) The rCBV within $FLAIR_{ROI}$ and $FDOPA_{ROI}$ are significantly higher in IDH_{wt} than in IDH_m gliomas. d) The ADC within $FLAIR_{ROI}$ and $FDOPA_{ROI}$ are significantly lower in IDH_{wt} than in IDH_m gliomas. e) ROC curves show the best AUC to differentiate IDH status when using $FDOPA_{ROI}$ and $nSUV_{max}$ (AUC 0.91, sensitivity 84%, specificity 87%). *, **, and *** mean $P < 0.05$, < 0.01, and < 0.001, respectively

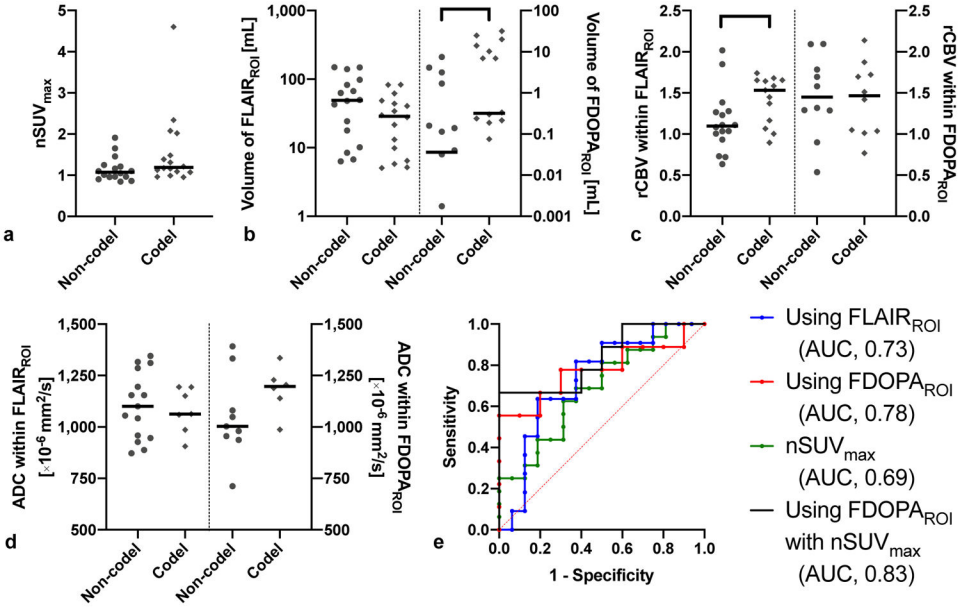

Fig. 3.

Imaging metrics of FDOPA PET and MRI, and ROC curves in IDH_m 1p19q codeleted (n = 16) and non-codeleted gliomas (n = 16). a) The $nSUV_{max}$, b) volume of $FLAIR_{ROI}$ and $FDOPA_{ROI}$, c) rCBV, and d) ADC are shown for different 1p19q codeletion statuses. Only FDOPA volume and rCBV within $FLAIR_{ROI}$ are significantly higher in 1p19q codel than non-codel gliomas. e) ROC curves show the best AUC to differentiate 1p19q codeletion status when using $FDOPA_{ROI}$ with $nSUV_{max}$ (AUC, 0.83; sensitivity, 67%; specificity, 90%). * means $P < 0.05$

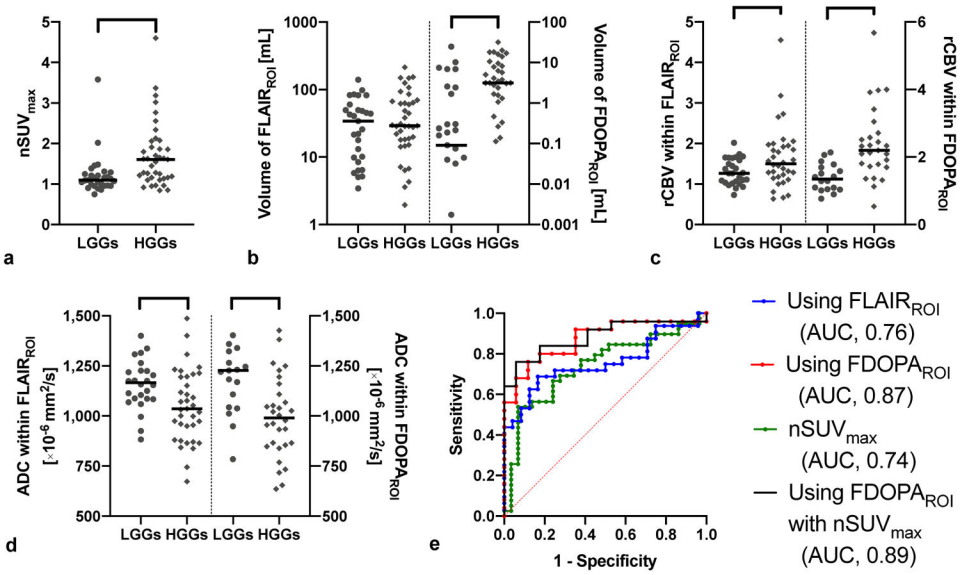

Fig. 4.

Imaging metrics of FDOPA PET and MRI, and ROC curves in LGGs (n = 29 grade II) and HGGs (n = 39 grade III and IV). a) The $nSUV_{max}$ and b) the $FDOPA_{ROI}$ volume are significantly higher in HGGs than in LGGs. c) The rCBV within $FLAIR_{ROI}$ and $FDOPA_{ROI}$ are significantly higher in HGGs than in LGGs. d) The ADC within $FLAIR_{ROI}$ and $FDOPA_{ROI}$ are significantly lower in HGGs than in LGGs. e) ROC curves show the best AUC to differentiate IDH status when using $FDOPA_{ROI}$ with $nSUV_{max}$ (AUC, 0.89; sensitivity, 76%; specificity, 94%). *, **, and *** mean $P < 0.05$, < 0.01, and < 0.001, respectively

Table 1.

Patient demographics and molecular information

No. of patients		68			
Female		26 (38%)			
Age ± standard deviation (year)		51.7 ± 14.9			
WHO grade			II 29 (43%)	III 25 (37%)	IV 14 (21%)
IDH mutation and 1p19q codeletion status	Wild-type	36 (52%)	7	15	14
	Mutant 1p19q non-codeleted	16 (24%)	10	6	0
	Mutant 1p19q codeleted	16 (24%)	12	4	0
MGMT promoter methylation status	Unmethylated	27 (40%)	9	11	7
	Methylated	27 (40%)	11	10	6
	Unknown	14 (21%)	9	4	1
EGFR amplification status	Negative	38 (56%)	16	14	8
	Positive	11 (16%)	1	6	4
	Unknown	19 (28%)	12	5	2

IDH, isocitrate dehydrogenase; MGMT, O6-methylguani DNA methyltransferase; EGFR, epidermal growth factor receptor.